Phase coexistence and Landau expansion parameters for a $0.70Pb(Mg_{1/3}Nb_{2/3})O_3$-$0.30PbTiO_3$ single crystal

Hangbo Zhang,[1] Xiaoyan Lu,[1,*] Ruixue Wang,[2] Chunying Wang,[2] Limei Zheng,[2] Zhen Liu,[2] Chao Yang,[2] Rui Zhang,[2] Bin Yang,[2] and Wenwu Cao[2,3,†]

[1]*School of Civil Engineering, Harbin Institute of Technology, Harbin 150001, China*

[2]*Condensed Matter Science and Technology Institute, Harbin Institute of Technology, Harbin 150080, China*

[3]*Department of Mathematics and Materials Research Institute, The Pennsylvania State University, University Park, Pennsylvania 16802, USA*

(Received 7 December 2016; revised manuscript received 7 June 2017; published 14 August 2017)

Multidomain relaxor-based ferroelectric single crystals $(1\text{-}x)Pb(Mg_{1/3}Nb_{2/3})O_3$-$xPbTiO_3$ (PMN-PT) have extraordinarily large electromechanical properties, but the origin of their giant piezoelectric properties is still not well understood. The Landau-like phenomenological theory is a feasible tool to study domain structures and their correlation with piezoelectric effects, but so far no expansion coefficients have been measured due to the phase mixture complication involved. In this work, the Landau free-energy expansion parameters for $0.70Pb(Mg_{1/3}Nb_{2/3})O_3$-$0.30PbTiO_3$ (PMN-0.30PT) single crystal were determined from the temperature-dependent polarization-electric field (P-E) hysteresis loops along $[001]_C$ and $[011]_C$ directions, and the rhombohedral (R) to tetragonal (T) phase-transition temperature. Using the obtained parameters, ferroelectric and dielectric properties were quantitatively calculated and compared with experiments. Good agreement was achieved in the temperature regions of T and R phases, but deviations were found in the cubic-phase temperature region since the contribution of polar nanoregions was not considered. In the phase-coexistence region from 73 to 93 °C, the polarization and dielectric constant can be quantitatively explained with the volume fractions of the coexisting R and T phases predicted by the canonical distribution. These obtained parameters can help theoretical studies and simulations of these relaxor-based ferroelectric single crystals to reveal the correlation between domain microstructures and the origin of giant electromechanical properties of multidomain PMN-PT single crystals.

DOI: 10.1103/PhysRevB.96.054109

I. INTRODUCTION

Relaxor-based ferroelectric single crystals with remarkable electromechanical performance have been extensively studied over the past two decades owing to their wide applications in ultrasonic medical imaging, large strain actuators, sensors, and other electromechanical devices [1–3]. In particular, [001] direction poled $(1\text{-}x)Pb(Mg_{1/3}Nb_{2/3})O_3$-$xPbTiO_3$ (PMN-xPT) single crystals with engineered domain structures show giant piezoelectric response ($d_{33} > 2000\,pC/N$) and very high electromechanical coupling factor ($k_{33} > 90\%$). The highest piezoelectric properties were found in compositions near the morphotropic phase boundary (MPB), i.e., with the PT content ranging from about 0.31 to 0.35 [4–8]. The large effective piezoelectric response was attributed to the easy rotation of polarization in the MPB composition, in which rhombohedral (R) and tetragonal (T) phases coexist or bridging monoclinic (M) phases appear [9–11].

The Landau thermodynamic theory has been proven effective to study the dielectric and piezoelectric responses, as well as the polarization rotation and domain formation in classical ferroelectrics, such as $BaTiO_3$ and $PbTiO_3$ [12–14]. However, there is still no quantified Landau free energy to describe the relaxor-based ferroelectrics for better understanding of their physical properties. Although the Landau theory failed to describe diffusive dielectric properties in relaxor ferroelectrics because of the polar nanoregions, it still can be adopted to describe the behaviors of relaxor-based ferroelectrics in the ferroelectric states, i.e., it works well in the temperature region below the paraelectric-ferroelectric phase transition. The challenge is to experimentally determine the expansion coefficients because two phases usually coexist in the MPB compositions. To date, there are only two attempts in the literature on this issue, but the theoretical predictions based on those published Landau parameters did not fit well with experimental results [15,16]. In general, the Landau expansion parameters can be extracted from typical polarization switching behaviors around phase-transition temperatures, since the P-E loops show different features as the crystal goes through a field-driven phase transition [17,18]. For example, typical double-hysteresis loops exist around the paraelectric-ferroelectric phase-transition temperature, which can be used to extract the parameters along the $[001]_C$ direction [19,20]. Other parameters can also be fitted by using the Landau expansions along particular orientations. In principle, we could cut crystals along the $[001]_C$, $[011]_C$, and $[111]_C$ directions to extract the complete set of Landau expansion parameters, but the task involves many technical complications and uncertainties.

In order to meet the theoretical conditions, single-domain state must be used to avoid contributions of internal stresses and domain walls. For crystals with $[001]_C$ orientation, we applied a high electric field (usually larger than two times the coercive field) near the tetragonal to cubic (C) phase-transition temperature to avoid the presence of tetragonal a/c domains. Similarly, we induced tetragonal to orthorhombic (O) phase transition using a large field along the $[011]_C$ direction. For the rhombohedral phase, it is almost pure in the temperature

*luxy@hit.edu.cn
†dzk@psu.edu

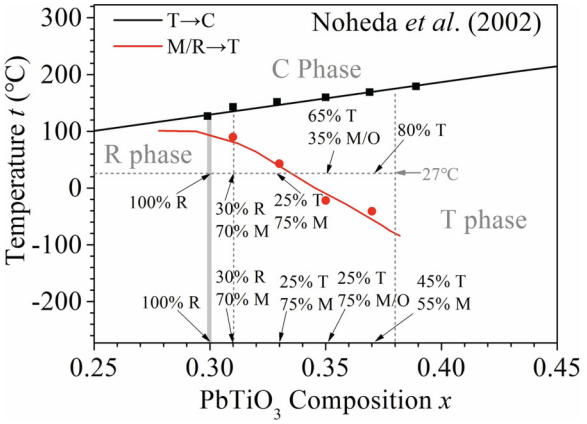

FIG. 1. Phase diagram of PMN-xPT system given by Noheda *et al.* [8].

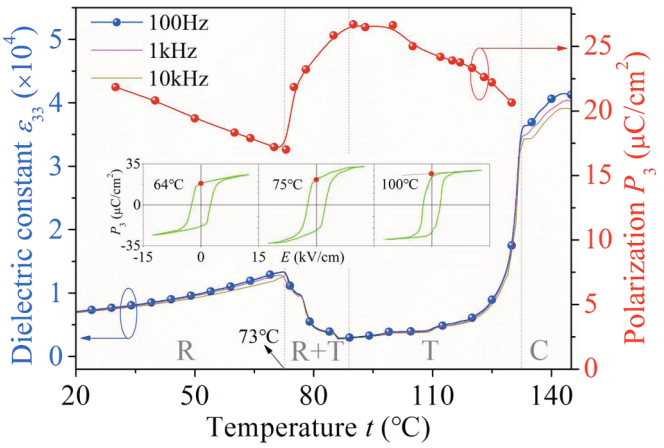

FIG. 2. Temperature-dependent polarization and dielectric constant at different frequencies. Inset figures are hysteresis loops along $[001]_C$ at temperatures of 64, 75, and 100 °C.

region from −250 °C to room temperature for the PMN-0.30PT according to the phase diagram as shown in Fig. 1 [8], which can be used for extracting the parameters related to the $[111]_C$ direction [21]. Thus, a set of Landau expansion parameters for PMN-0.30PT can be obtained by analyzing the double loops around the cubic to tetragonal and orthorhombic, and tetragonal to rhombohedral phase transitions. To verify the obtained parameters, we calculated the dielectric constant and polarization in a wide range of temperature within the ferroelectric phase state and compared with experimental results. Finally, the room-temperature orientation-dependent piezoelectric responses were theoretically calculated and compared with experimental results.

II. EXPERIMENTS AND FITTING PROCEDURE

The PMN-0.30PT single crystal was grown by the modified Bridgeman method, and the samples were oriented by the Laue x-ray machine and cut into 4 mm × 4 mm × 0.5 mm plates. To eliminate the oxygen defects, all the samples were annealed at 600 °C for 1 h before further processing. The PT content was defined by comparing the Curie temperature t_c with the phase diagram given by the synchrotron x-ray powder diffraction [8]. Two kinds of plates were prepared. One (plate #1) is for the measurement of dielectric constant ε_{33} and P-E loops along the $[001]_C$ direction with gold electrodes sputtered onto the $(001)_C$ faces. The other (plate #2) is poled along the $[110]_C$ direction with gold electrodes on the $(110)_C$ faces. To measure the dielectric property, plate #1 was poled under an electrical field of 15 kV/cm for 15 min at room temperature. Domain configurations were determined by polarizing light microscopy (Zeiss Axiokop40) with crossed polarizer/analyzer (P/A) pairs based on the extinction position of the domains and the orientation of the domain walls. The dielectric constant ε_{33} was measured from room temperature to 200 °C using an LCR meter (Agilent, E4980A) with the heating rate of 2 °C/min at frequencies of 100 Hz, 1 kHz, and 10 kHz. After the measurement of dielectric constants, the crystal was slowly cooled down to room temperature, then put into a silicon oil bath for the measurement of the P-E loops using the Precision Premier II system (Radiant Tech, USA). For both samples, the tested electric field is sinusoidal with the maximum field magnitude of 10 kV/cm at 0.1 Hz, which ensures the polarization to be fully reversed in each cycle. Verifications of the single-domain states for these samples are given in the Appendix. The temperature-increasing steps were set differently near and far away from the phase-transition temperatures. From room temperature to 65 °C, the temperature step was 5 °C; around the R-T phase-transition temperature of 73 °C, i.e., from 65 to 75 °C, the temperature step was 1 °C; from 75 to 120 °C, the temperature step was 5 °C. Near the tetragonal to cubic phase-transition temperature of about 132 °C, i.e., from 120 to 145 °C, the temperature step was 1 °C. All data were recorded after the temperature in the oil bath became stable.

The Landau phenomenological theory with the free energy up to sixth-order expansions in polarization was used in this work. We should note that although free energy with eighth-order expansions is needed to allow the presence of M phases, it is not possible to determine uniquely the eighth-order expansion coefficients using available experiments. Furthermore, both the R and T phases can be easily distorted to M-like phases due to internal stresses from the interface mismatch of coexisting phases, so M phases may not be an intrinsic phase [22]. We found that it is sufficient to describe all experimental phenomena in the ferroelectric state using the free energy up to the sixth-order expansion Landau theory.

The temperature-dependent polarization and dielectric constant of a $[001]_C$ poled PMN-0.30PT single-crystal plate were measured in the heating process. As shown in Fig. 2, there are four temperature regions, corresponding to different polarization and dielectric susceptibility states. Here, we mainly focus on the ferroelectric state, i.e., the R state, T state, and coexistence of R and T states. The inset figures are hysteresis loops along $[001]_C$ at different temperatures. At 64 and 100 °C, the crystal shows typical loops of R and T phases, respectively. At 75 °C, the crystal shows a phase transition under a large electric field, which indicates the rotation of polarization from $[111]_C$ to $[001]_C$. The measured phase-transition temperatures were slightly different because two isolated measurement systems were used, although they

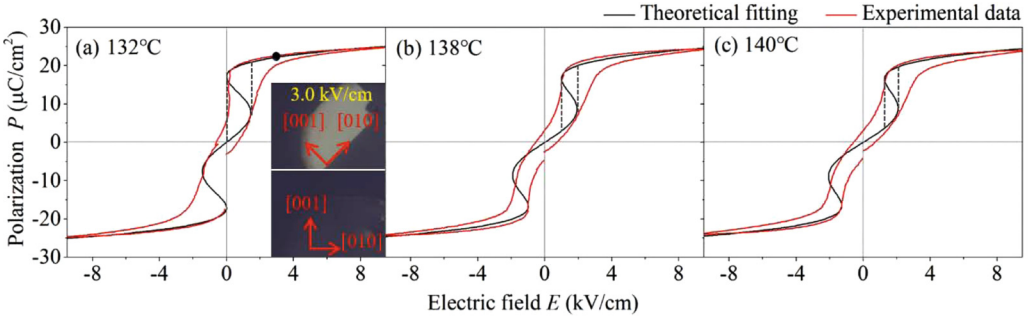

FIG. 3. Theoretical fittings of $[001]_C$-oriented PMN-0.30PT hysteresis loops at temperatures of (a) 132 °C, (b) 138 °C, and (c) 140 °C. Single-domain state at 132 °C was verified by using the polarizing light microscopy as inset in (a).

matched quite well over the whole measured temperature range.

A. Double-hysteresis loops along $[001]_C$

Since the Landau parameters can be determined from typical polarization switching behaviors around the phase-transition temperatures, we will first focus on the electric-field-induced double-hysteresis loops around the $T \rightarrow C$ phase transition temperature (t_c). As expected, the crystal (plate #1) showed a typical single loop under an electric field below the phase-transition temperature. When the temperature approached t_c, double loops were observed. In our case, the double loop initially occurred at $t_1 = 132\,^{\circ}\mathrm{C}$, at which the cubic phase was transformed into the tetragonal phase by the applied electric field [11]. For the tetragonal phase, the free energy can be simplified as a function of the polarization component P_3:

$$G_{001} = \alpha_1 P_3^2 + \alpha_{11} P_3^4 + \alpha_{111} P_3^6 - E_3 P_3. \quad (1)$$

The relationship between the applied electric field E_3 and the polarization P_3 along $[001]_C$ can be expressed as

$$E_3 = \partial G_{001}/\partial P_3 = 2\alpha_1 P_3 + 4\alpha_{11} P_3^3 + 6\alpha_{111} P_3^5. \quad (2)$$

The observed double-hysteresis loops in a certain temperature range indicate the contributions of high-order terms as shown in Fig. 3. The final single-domain states at different temperatures under a large electric field were verified by using the polarizing light microscopy (PLM) as described in the Appendix. Since all results are similar, PLM results at 132 °C under an electric field of 3 kV/cm were inset in Fig. 3(a) as a showcase. Because the behavior of polarization with respect to the electric field is determined by the coefficients α_1, α_{11}, and α_{111}, those double-hysteresis loops can be used to obtain these three coefficients by fitting the measured loops. The obtained parameters at different temperatures are listed in Table I. Here, α_1 is linearly dependent on temperature and can be expressed as $\alpha_1 = \alpha_0(t - t_0)$, with $\alpha_0 = 0.745 \times 10^5 (\mathrm{m/F\,^{\circ}C})$, where t and t_0 are ambient temperature and Curie-Weiss temperature, respectively. The corresponding Curie constant is $C_r = 1/2\varepsilon_0\alpha_0 = 7.584 \times 10^5\,^{\circ}\mathrm{C}$, which is of the same order of magnitude for displacive ferroelectrics [23]. The parameters α_{11} and α_{111} are almost temperature independent.

TABLE I. Parameters obtained by fitting the $[001]_C$ loops of PMN-0.30PT at three typical temperatures.

t (°C)	132	138	140
$\alpha_1(10^6\,\mathrm{m/F})$	1.470	1.832	2.033
$\alpha_{11}(10^8\mathrm{m}^5/\mathrm{C}^2\mathrm{F})$	−0.5000	−0.5000	−0.5025
$\alpha_{111}(10^9\mathrm{m}^9/\mathrm{C}^4\mathrm{F})$	0.5567	0.5571	0.5567

B. Hysteresis loops along $[011]_C$

The parameters α_{12} and α_{112} cannot be obtained in the orthorhombic phase with the assistance of electric field along $[011]_C$ at a temperature slightly higher than t_C. Thus, we heated plate #2 up to 120 °C with a temperature step of 5 °C, then with a temperature step of 1 °C when the temperature is higher than 120 °C. Typical hysteresis loops obtained from plate #2 are shown in Fig. 4. In order to reach the single-domain state, we applied an electric field large enough to make sure that the O phase appears in the hysteresis loop. We should note that the polarization vector in the T phase is smaller than that in the O phase, which can be used to verify the phase state. Additional verification of the single-domain state was carried out using PLM as shown in the Appendix. Results at 132 °C under an electric field of 3.5 kV/cm were selected as a showcase and inset in Fig. 4(c).

At 128 °C, the crystal is in the tetragonal state when the applied electric field is lower than 0.4 kV/cm. Under the electric field of 0.4 kV/cm, the crystal goes through a very sharp $T \rightarrow O$ phase transition. With further increase of the electric field, stable O phase state gradually formed as shown in Fig. 4(a). With the increase of temperature, the T phase becomes unstable and suddenly disappears at the critical temperature, as what happened in the $[001]_C$ case. At 132 °C, PMN-0.30PT shows the typical P-E curve for an initial T phase and a sudden T-O phase transition with the assistance of a large electric field along $[011]_C$. The zero-field polarization along $[011]_C$ at 132 °C is 13.35 μC/cm^2, about $1/\sqrt{2}$ of $[001]_C$ polarization (18.30 μC/cm^2), which indicates the initiation of the tetragonal phase at this stage. With further increase of the temperature, paraelectric phase dominates, but field-induced phases can also be formed. As shown in Fig. 4(c), at 137 °C the formed O phase indicates a direct transition from the cubic to orthorhombic phase. By numerically fitting the induced O phase data, two combinations of Landau expansion parameters can be obtained: $\alpha_{11}^{O} = 0.3781 \times 10^8\mathrm{m}^5/\mathrm{C}^2\mathrm{F}$ and $\alpha_{111}^{O} = 0.4724 \times 10^9\mathrm{m}^9/\mathrm{C}^4\mathrm{F}$, respectively [19]. Then,

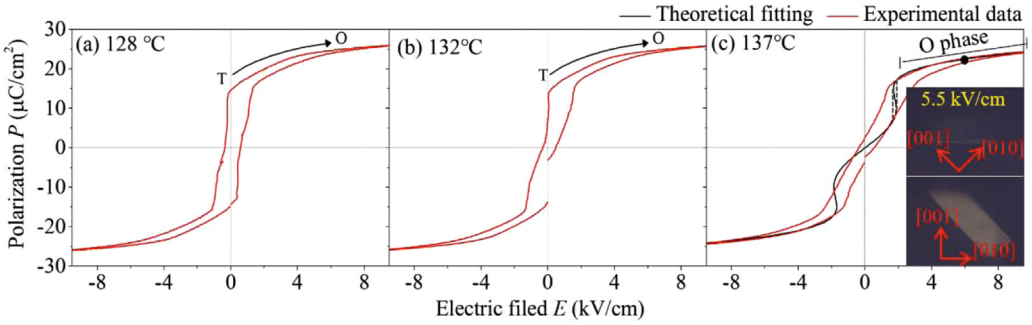

FIG. 4. Hysteresis loops of $[011]_C$-oriented PMN-0.30PT at (a) 128 °C, (b) 132 °C, and (c) 137 °C. Single-domain state at 137 °C was verified by using the polarizing light microscopy as inset in (a).

from the relations of $\alpha_{11}^{O} = \frac{1}{2}\alpha_{11} + \frac{1}{4}\alpha_{12}$ and $\alpha_{111}^{O} = \frac{1}{4}(\alpha_{111} + \alpha_{112})$, we can extract the two expansion parameters $\alpha_{12} = -0.5125 \times 10^8 \mathrm{m}^5/\mathrm{C}^2\mathrm{F}$ and $\alpha_{112} = 1.3333 \times 10^9 \mathrm{m}^9/\mathrm{C}^4\mathrm{F}$.

C. Parameter α_{123} determined by $R \rightarrow T$ phase transition

Following the same procedure, α_{123} was supposed to be found in the $[111]_C$-oriented hysteresis loops. To decrease the number of used samples, we use an alternative way, which is to numerically equate the free energies of the R and T phases following the same method adopted by Haun *et al.* [24]. In plate #1, the $R \rightarrow T$ phase transition temperature obtained from the remnant polarization-temperature curve is about 73 °C as shown in Fig. 2, which is close to the value given by the phase diagram ($t_{R\text{-}T} = 77$ °C) [8]. Since 73 °C is a phase-transition temperature from fully poled $4R$ state to newly formed $1T$ phase state, it is a rather sharp phase transition, as illustrated in the polarization and dielectricity curves in Fig. 2. The parameter α_{123} thus was determined to be $0.24 \times 10^9 \mathrm{m}^8/\mathrm{C}^4\mathrm{F}$ by equating the free energies of the R and T phases at 73 °C.

III. LANDAU PHENOMENOLOGICAL MODEL

In order to verify the obtained expansion parameters, we calculated the polarization and dielectricity in a wide range of temperature based on the Landau phenomenological theory with the parameters determined only by the high-temperature hysteresis loops and R-T phase-transition temperature of 73 °C. Under an external electric field $\boldsymbol{E}$ of arbitrary direction, the classical Landau-Devonshire free-energy expansions with internal stress X_i and polarization P_i as the primary and secondary order parameters can be expressed as [22,24]

$$\begin{aligned} G = {} & \alpha_1\left(P_1^2 + P_2^2 + P_3^2\right) + \alpha_{11}\left(P_1^4 + P_2^4 + P_3^4\right) \\ & + \alpha_{12}\left(P_1^2P_2^2 + P_2^2P_3^2 + P_3^2P_1^2\right) \\ & + \alpha_{111}\left(P_1^6 + P_2^6 + P_3^6\right) + \alpha_{112}\left[P_1^2\left(P_2^4 + P_3^4\right)\right. \\ & \left. + P_2^2\left(P_3^4 + P_1^4\right) + P_3^2\left(P_1^4 + P_2^4\right)\right] + \alpha_{123}P_1^2P_2^2P_3^2 \\ & - \tfrac{1}{2}s_{11}\left(X_1^2 + X_2^2 + X_3^2\right) - s_{12}(X_1X_2 + X_2X_3 + X_3X_1) \\ & - \tfrac{1}{2}s_{44}\left(X_4^2 + X_5^2 + X_6^2\right) - Q_{11}\left(X_1P_1^2 + X_2P_2^2 + X_3P_3^2\right) \\ & - Q_{12}\left[X_1\left(P_2^2 + P_3^2\right) + X_2\left(P_3^2 + P_1^2\right) + X_3\left(P_1^2 + P_2^2\right)\right] \\ & - Q_{44}(X_4P_2P_3 + X_5P_1P_3 + X_6P_2P_1) \\ & - E_1P_1 - E_2P_2 - E_3P_3, \end{aligned} \tag{3}$$

where s_{ij} and Q_{ij} are the elastic compliances and electrostrictive coefficients, respectively. The elastic compliances s_{ij} for PMN-0.30PT were taken from Ref. [25].

The electrostrictive coefficients Q_{ij} for $x = 0.30$ can be obtained by fitting the spontaneous strains to the values given by the synchrotron x-ray powder diffraction [8] with obtained polarization. The strains in the tetragonal phase are $S_1 = S_2 = Q_{12}\,P_3^2$, $S_3 = Q_{11}\,P_3^2$, and $S_4 = Q_{44}\,P_3^2$, corresponding to the strain $S_1 = S_2 = (a_T - a_C')/a_C'$, $S_3 = (c_T - a_C')/a_C'$, and $S_4 = 1 - \frac{\alpha}{90}$ given by the synchrotron x-ray powder diffraction, respectively [21,24]. a_T and c_T are the lattice constants of the tetragonal structure, a_C' is the lattice constant of the cubic structure extrapolated into the tetragonal region, and α is the tilting angle of the crystal structure [21,23]. The obtained temperature-independent electrostrictive coefficients are $Q_{11} = 0.055\mathrm{m}^4/\mathrm{C}^2$, $Q_{12} = -0.023\mathrm{m}^4/\mathrm{C}^2$, and $Q_{44} = 0.0315\mathrm{m}^4/\mathrm{C}^2$, which are in good agreements with the results given in Ref. [26] with $Q_{11} = 0.0555\mathrm{m}^4/\mathrm{C}^2$ and $Q_{12} = -0.023\mathrm{m}^4/\mathrm{C}^2$ for the T phase, and $Q_{44} = 0.020\mathrm{m}^4/\mathrm{C}^2$ for R phase of room-temperature PMN-0.30PT. The value of Q_{44} in our fitting is about 1.58 times the value in Ref. [26]. The difference may come from the different polarization of the R phase at room temperature. The polarization given in Ref. [26] is about 24 $\mu\mathrm{C/cm}^2$, which is higher than our results (about 22 $\mu\mathrm{C/cm}^2$ from our experiment and 20 $\mu\mathrm{C/cm}^2$ from the theoretical calculation). With the obtained electrostrictive coefficients, the comparison between theoretical fittings and experimental values of normal strains S_1, S_2, and shear strain S_4 are given in Fig. 5, and are in good agreement. Due to the lack of experimental results on the temperature-dependent strain, the elastic compliances were taken from Ref. [26]. All parameters used for PMN-0.30PT are listed in Table II.

Up to now, we extracted the full set of the six-order Landau free-energy expansion parameters directly using the high-temperature P-E hysteresis loops along the $[001]_C$ and $[011]_C$ directions and the rhombohedral (R) to tetragonal (T) phase-transition temperature. The electrostrictive coefficients were obtained by fitting the strain given by the synchrotron x-ray powder diffraction and the polarization measured in our experiments, and also verified with the results obtained by using the resonance method.

In the next section, the polarization and dielectricity in the whole temperature range will be calculated and compared with

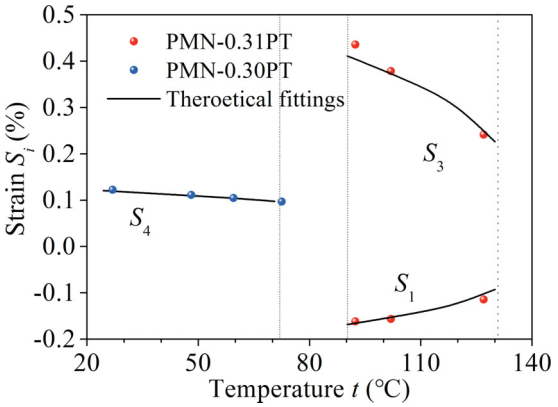

FIG. 5. Experimental and theoretical calculated strains for PMN-0.30PT and PMN-0.31PT single crystals.

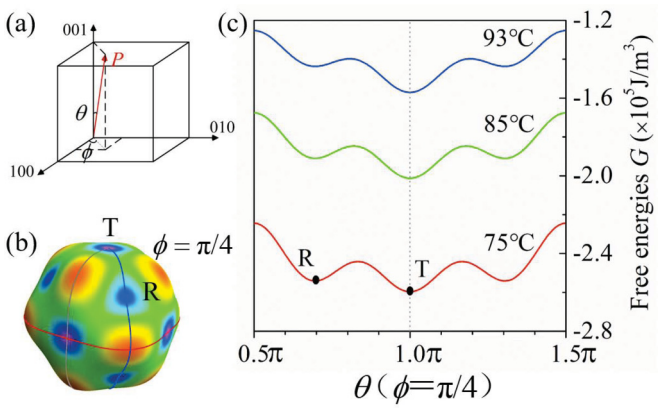

FIG. 6. (a) Schematic of arbitrary spatial polarization as a function of angles θ and φ, (b) energy surface of coexisting R and T phases, and (c) the angular variation of free energy of R and T phase at 75, 85, and 93 °C.

the experimental results. In addition, phase coexistence in the temperature range from 73 to 93 °C will be considered with an estimation of the existing R and T volume fractions.

IV. PHASE COEXISTENCE AND PHYSICAL PROPERTIES

The polarization vector in different ferroelectric states can be determined by using the equilibrium conditions $\partial G/\partial P_i = 0$ ($i = 1,2,3$). As illustrated in Ref. [22], there is an obvious phase-coexisting region near the phase transition, especially for phases with similar free energies. In this case, R and T phases may coexist in the temperature range from 73 to 93 °C since significant differences between the calculated results and the experimental results were observed. To better understand the increase of the dielectric constant and the decrease of polarization, we first verified the phase stability using the Hessian matrix [27,28], and calculated the free-energy surfaces with coexisting R and T phases as shown in Fig. 6. With an arbitrary spatial polarization as a function of angles θ and φ [as schematically shown in the inset of Fig. 6(a)], the coexistence of R and T phases was confirmed in the energy surface [Fig. 6(b)]. To better illustrate the phases' coexistence, the representative free-energy surfaces in the (110) plane ($\varphi = \pi/4$) as a function of angle θ ($0.5 \leqslant \theta \leqslant 1.5\pi$, where $\theta = 0$ corresponds to the $[001]_C$ direction) are shown in Fig. 6(c) at various temperatures, which illustrates the coexistence of R and T phase at 75 °C and the instability of the R phase with the increase of temperature. At 93 °C, the energy profit is flatter than those at 75 and 85 °C, indicating a lower phase-transition barrier between the T and R phases. In this case, the R phase is metastable and can be easily rotated into the T phase by an external field [29].

To better describe the physical properties, phase-volume ratio should be estimated for the phase-coexisting region from 73 to 93 °C. Based on the canonical distribution within the framework of statistical mechanics, the distribution function of the unit cell being in the energy level E_i can be written as [22]

$$\gamma_i \propto \exp\left(-\frac{G_i V_i - G_0 V_0}{kt}\right), \tag{4}$$

where k is the Boltzmann constant, t is temperature. G_i is the system free-energy densities for the ith low-temperature structural phase with volume V_i. G_0 and V_0 are the ground-state energy density and volume, respectively. The volume V_i refers to the occupation of each phase and can be expressed as $V_i = n_i v_i$, with n_i being the total number of unit cells for each domain, and v_i the volume of each cell. We first consider the R and T phases in PMN-0.30PT. The volume fraction is $f_i = \gamma_i/(\gamma_R + \gamma_T)$ with $f_R + f_T = 1$ ($i = R$, T refers to R and T phases, respectively).

The distribution function is exponentially dependent on the volume size and free-energy density of each phase, which is highly temperature dependent as shown in Fig. 7. For simplicity, we consider the same domain size for the two phases. Volumes containing different unit cells also affect the ratio of R and T phase fractions. Smaller volume shows larger coexisting probability in a larger temperature range. In this case, the R phase disappears around 93 °C; thus, a volume containing 35 000 u.c. was used for further calculations, which corresponds to a 13-nm cube.

With the predicted volume fraction and volume size, the dielectric constant and polarization in the temperature range of 73 to 93 °C were calculated. Together with the results for the single-domain states in other temperature ranges, the dielectric constant and polarization were calculated and compared with experimental results as shown in Fig. 8. In

TABLE II. Landau parameters and tetragonal phase elastic constants s_{ij} and Q_{ij}.

Parameters of PMN-0.30PT			
t_0 (°C)	112.7 °C	Q_{11} (m^4/C^2)	0.055
C(10^5 °C)	7.584	Q_{12} (m^4/C^2)	−0.023
α_0(10^5 m/F°C)	0.745	Q_{44} (m^4/C^2)	0.0315
α_1(10^5 m/F)	0.745×(t − 112.7 °C)	s_{11} (10^{-12}m^2/N)	39.7
α_{11}(10^8m^5/C^{2}F)	−0.5000	s_{12} (10^{-12}m^2/N))	− 32.1
α_{12}(10^8m^5/C^{2}F)	−0.5125	s_{13} (10^{-12}m^2/N)	− 4.7
α_{111}(10^9m^9/C^{4}F)	0.5567	s_{33} (10^{-12}m^2/N)	10.8
α_{112}(10^9m^9/C^{4}F)	1.333	s_{44} (10^{-12}m^2/N)	12.9
α_{123}(10^9m^9/C^{4}F)	0.24	s_{66} (10^{-12}m^2/N)	15.2

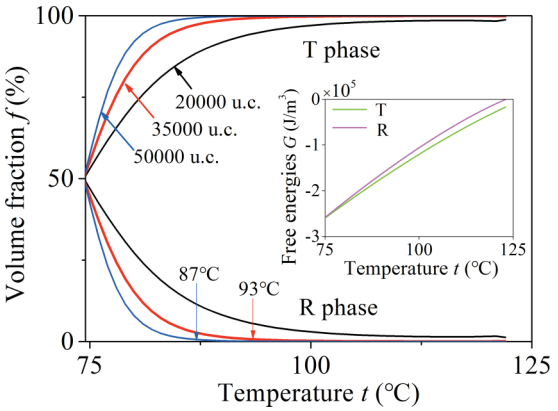

FIG. 7. Distribution fractions for tetragonal and rhombohedral phases from 73 to 125 °C with volumes containing n unit cells (u.c.) and $n = 20\,000$, 35 000, and 50 000.

the whole temperature range, the theoretical results fit well with the experimental data except the slightly lower theoretical value of P_3 in the R phase compared with the experimental values. We should note that the $[001]_C$ poled crystal at low temperatures is in the $4R$ state with four symmetrically distributed R domains around $[001]_C$. If the domain size is big enough and domain wall contributions can be neglected, the dielectric constant ε_{33} of the $1R$ state along $[001]_C$ would be the same as the results for the $4R$ state along $[001]_C$; thus,

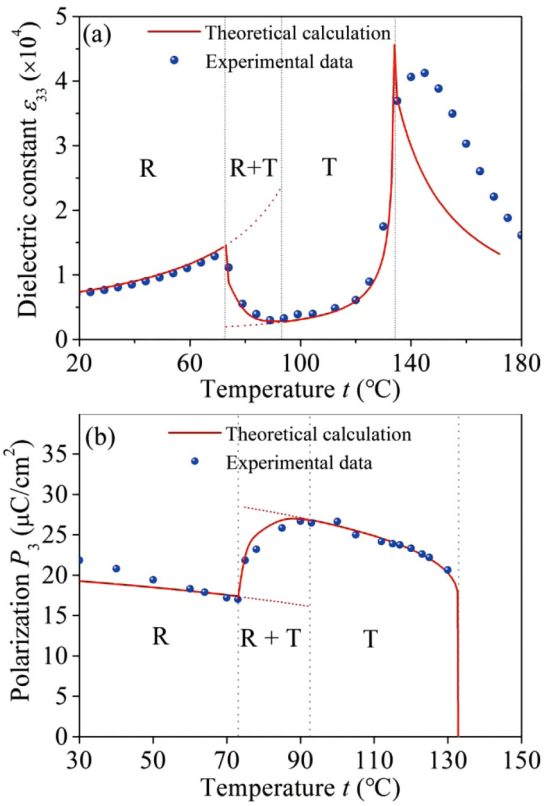

FIG. 8. Comparison between theoretical calculations and experimental results. (a) Dielectric constant ε_{33} and (b) spontaneous polarization P_3.

TABLE III. Orientation-dependent piezoelectric coefficients at room temperature.

d_{ij} (pC/N)	d_{33}	d_{31}	d_{15}
Theory (this work)	1860	−910	141
Experiments [25]	1981	−921	190

the theoretical calculation can be directly compared with the experimental results.

The room-temperature anisotropic piezoelectric coefficients d_{ij} were also calculated and compared with the experimental values as shown in Table III. All three predicted piezoelectric constants are in good agreement with experimental results of Ref. [25]. We also calculated the d_{33}^R in the rhombohedral crystallographic coordinates [30], which was about 106 pC/N, comparable but larger than the experimental result of about 80 pC/N [31].

V. SUMMARY AND CONCLUSIONS

The Landau expansion parameters for the PMN-0.30PT single crystal have been obtained by fitting the hysteresis loops and analyzing the $R \rightarrow T$ phase-transition temperature. Using the experimentally obtained parameters, polarization and dielectric response have been calculated, which are in quantitative agreement with experimental values. In the phase-coexisting temperature range, the R phase is metastable and could be easily rotated by an external field, which will help generate large piezoelectric responses. Although the relaxor nature could not be described by the Landau theory in the cubic phase, our work here shows that the Landau theory works well for the ferroelectric R and T phases, in which the polar nanoregions are being aligned with the spontaneous polarization field. The complete set of Landau expansion parameters we obtained in this work will greatly facilitate the simulation studies on the domain formation and domain dynamics in the PMN-xPT single crystals and could help us quantitatively link the giant piezoelectric properties with domain size and domain wall contributions.

ACKNOWLEDGMENTS

This research was supported by the National Science Foundation of China (Grants No. 11372002 and No. 51572055), the National Basic Research Program of China (Grant No. 2013CB632900), and the PIRS of HIT (Grant No. B201509).

APPENDIX

In order to determine reliable expansion parameters of the free energy by fitting the saturated D-E loop within the framework of the Landau theory, samples must be in single domain of pure phase. In our experiments, the single-domain states of PMN-PT single crystals were verified by using the polarizing light microscopy based on the birefringence of crystals. To observe the domain structures under certain temperatures or applied electric fields, we used PLM (Zessi Axioskop 40) equipped with a heating-cooling optical stage

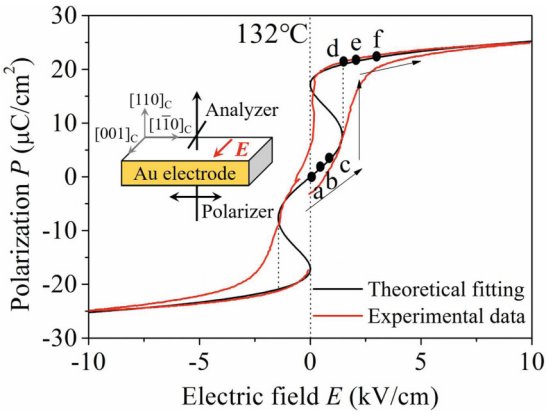

FIG. 9. P-E hysteresis loop at 132 °C. Inset is the illustration of the sample with crossed analyzer/polarizer pairs and the applied electric field direction.

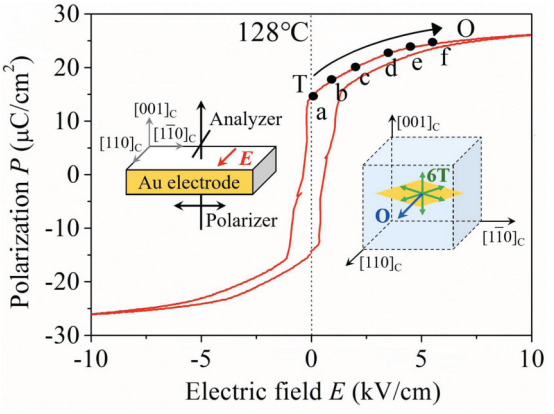

FIG. 11. P-E hysteresis loop at 128 °C. Left inset is the illustration of the sample #2 with crossed analyzer/polarizer pairs and the applied electric field direction. Right inset is the polarization state from $6T$ state to $1O$ state.

(LINKAM THMS 400) and a dc source with a dc bias fixture (Agilent 16065A).

When a single-domain crystal is placed in between the mutually perpendicular polarizer and analyzer, the transmitted light intensity is given by

$$I = I_0 \sin^2 2\alpha \sin^2 \frac{\phi}{2}, \tag{A1}$$

where I_0 is the amplitude of the transmitted light intensity, a is the angle between the polarizer and the projection of the optic axis, and ϕ is the phase angle, which is usually fixed, so that the transmitted light intensity depends only on the angle a. The extinction angles can tell the phase of the crystal and the intensity distribution can tell us if the crystal is in a single phase.

1. Phase hysteresis under an electric field along $[001]_C$

Both experiments and Landau theory show that a special double loop exists at a particular temperature t_1 under an electric field (Fig. 9). To probe the phase change under electric fields and verify the single-domain state of $[001]_C$ poled crystal at this temperature, a thin and slim plate (sample #1) with dimensions of 0.6 mm ∥ $[011]_C$ × 1.1 mm ∥ $[001]_C$ × 3.0 mm ∥ $[1\bar{1}0]_C$ was used as shown in the inset of Fig. 9. The two large surfaces were fine-polished for domain observations, then the sample was annealed at 350 °C for 1 h to

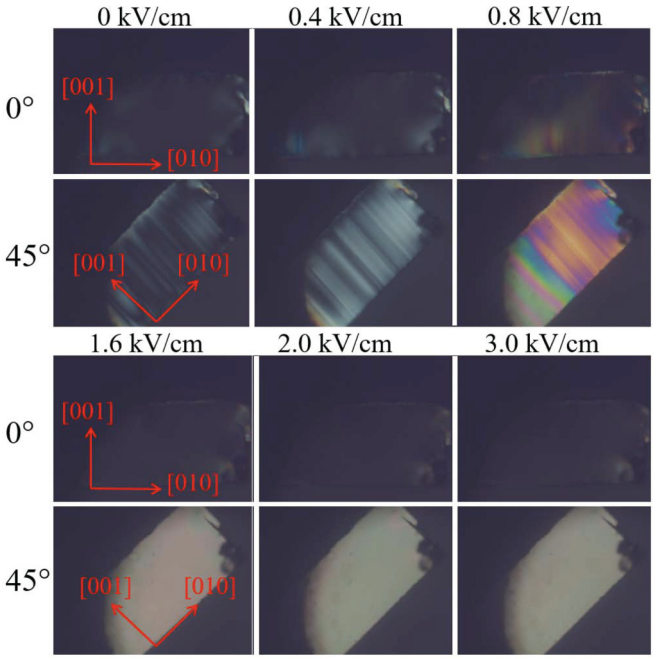

FIG. 10. Electric-field-dependent phase change at high temperature of 132 °C with a dc electric field applied along $[001]_C$ observed at the polarizer angle of 0 and 45°, respectively.

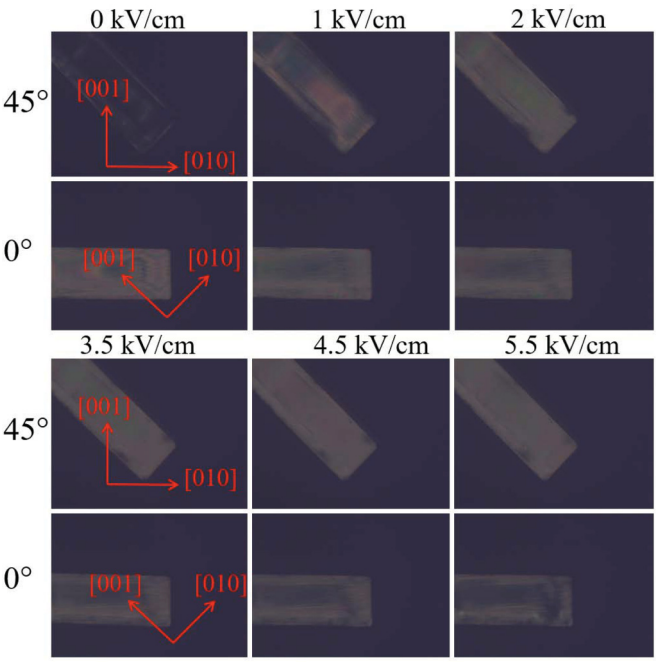

FIG. 12. Electric-field-dependent phase change at high temperature of 128 °C with a dc electric field applied along the $[001]_C$ direction observed at polarizer angle of 45 and 0°, respectively.

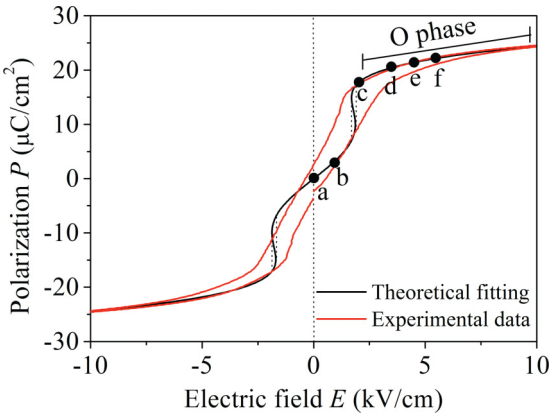

FIG. 13. P-E hysteresis loop at 137 °C.

eliminate the stresses induced by cutting and polishing. Gold film was vacuum sputtered onto the $[001]_C$ and $[00\bar{1}]_C$ surfaces as electrodes. The temperature was increased to 132 °C (above t_c) at a step of 5 °C and then kept there. The angle between the polarizer and the $[1\bar{1}0]_C$ direction was q. As shown in Fig. 10, complete extinction occurred in both 0 and 45° at zero field above 132 °C, indicating the initiation of the cubic phase. With the applied electric field increasing from zero to 3 kV/cm by a small step of 0.1 kV/cm, the tetragonal phase begins to form both in the in-plane and out-of-plane directions at the electric field amplitude of 0.4 kV/cm. When the electric field reached 1.6 kV/cm, the light intensity was the maximum, indicating the complete formation of tetragonal phase from the initial cubic phase. Such field-induced transition is rather sharp and the tetragonal phase can be kept under higher electric fields.

The field needed to form a stable T phase increases with the increase of temperature as predicted by the Landau theory. We have performed similar experiments at 138 and 140 °C, and the coercive fields of this sample are 1.6, 2.0, and 2.2 kV/cm at 132, 138, and 140 °C, respectively.

2. Phase hysteresis under an electric field along $[110]_C$

To verify the orthorhombic (O) single-domain state under an electric field along $[110]_C$, sample #2 with the size of 0.6 mm ∥ $[001]_C$ × 0.55 mm ∥ $[110]_C$ × 2.7 mm ∥ $[1\bar{1}0]_C$ was prepared and fine-polished, then annealed at 350 °C and kept 1 h without electric field. Gold electrodes were vacuum sputtered onto the $[110]_C$ and $[\bar{1}10]_C$ surfaces as shown in the left inset in Fig. 11. For easier PLM observation, the sample

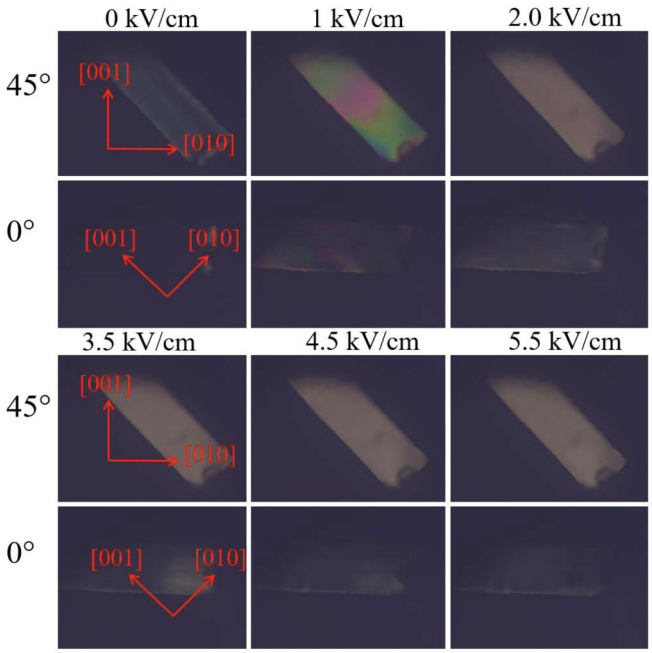

FIG. 14. Electric field dependence of domain structures at 137 °C with a dc electric field applied along $[011]_C$ observed at 45 and 0°, respectively.

was poled under an electric field of 0.2 k V/cm at 100 °C to switch the polarization into the in-plane tetragonal phase. The P-E hysteresis loop at 128 °C was measured as shown in Fig. 11.

At 128 °C, the T phase dominates as shown in Fig. 12 in which typical extinction for the in-plane T phase appeared. With the increase of electric field, the T phase changed to the O phase with a typical extinction angle for the O phase, which can be also seen in the P-E loops as shown in Fig. 11.

At 132 °C, which is above the phase-transition temperature t_c, the initial phase is cubic. Under a low electric field, extinction for the in-plane T phase along the electric field becomes dominant. With the increase of electric field along $[110]_C$, the O phase begins to form with bright in 0° and dark in 45°, indicating the formation of the O phase in a large area.

At even higher temperature of 137 °C, the O phase becomes easier to be induced as shown in Fig. 13. Complete extinction happens when the electric field reaches 5.5 kV/cm as shown in Fig. 14, indicating a complete formation of single-domain O phase.

[1] S. E. Park and T. R. Shrout, J. Appl. Phys. **82**, 1804 (1997).
[2] E. W. Sun and W. W. Cao, Prog. Mater. Sci. **65**, 124 (2014).
[3] L. M. Zheng, R. Sahul, S. J. Zhang, W. H. Jiang, S. Y. Li, and W. W. Cao, J. Appl. Phys. **114**, 104105 (2013).
[4] J. Luo and X. Geng, Prog. Mater. Sci. **68**, 1 (2015).
[5] R. Pirc and R. Blinc, Phys. Rev. B **76**, 020101 (2007).
[6] G. Xu, Z. Zhong, Y. Bing, Z. G. Ye, and G. Shirane, Nat. Mater. **5**, 134 (2006).
[7] E. V. Colla, N. K. Yushin, and D. Viehland, J. Appl. Phys. **83**, 3298 (1998).
[8] B. Noheda, D. E. Cox, G. Shirane, J. Gao, and Z. G. Ye, Phys. Rev. B **66**, 054104 (2002).

[9] M. Ahart, M. Somayazulu, R. Cohen, P. Ganesh, P. Dera, H. K. Mao, R. J. Hemley, Y. Ren, P. Liermann, and Z. Wu, Nature **451**, 545 (2008).
[10] A. K. Singh, D. Pandey, and O. Zaharko, Phys. Rev. B **74**, 024101 (2006).
[11] X. Y. Lu, L. M. Zheng, H. Li, and W. W. Cao, J. Appl. Phys. **117**, 134101 (2015).
[12] N. A. Pertsev, A. G. Zembilgotov, and A. K. Tagantsev, Phys. Rev. Lett. **80**, 1988 (1998).
[13] D. Damjanovic, Rep. Prog. Phys. **61**, 1267 (1998).
[14] B. V. Völker, C. M. Landis, and M. Kamlah, Smart Mater. Struct. **21**, 035025 (2012)
[15] J. H. Qiu, J. N. Ding, N. Y. Yuan, and X. Q. Wang, J. Appl. Phys. **117**, 074101 (2015).
[16] A. A. Heitmann and G. A. Rossetti, Jr., J. Am. Ceram. Soc. **97**, 1661 (2014).
[17] E. J. Huibregtse and D. R. Young, Phys. Rev. **103**, 1705 (1956).
[18] J. A. Gonzalo and J. M. Rivera, Ferroelectrics **2**, 31 (1971).
[19] X. Y. Lu, H. Li, and W. W. Cao, J. Appl. Phys. **114**, 224106 (2013).
[20] W. Merz, Phys. Rev. **91**, 513 (1953).
[21] O. Noblanc, P. Gaucher, and G. Calvarin, J. Appl. Phys. **79**, 4291 (1996).
[22] X. Y. Lu, H. B. Zhang, L. M. Zheng, and W. W. Cao, AIP Adv. **6**, 105208 (2016).
[23] F. Jona and G. Shirane, *Ferroelectric Crystals* (Dover, New York, 1993).
[24] M. J. Haun, E. Furman, S. J. Jang, H. A. McKinstry, and L. E. Cross, J. Appl. Phys. **62**, 3331 (1987).
[25] R. Zhang, W. H. Jiang, B. Jiang, and W. W. Cao, AIP Conf. Proc. **626**, 188 (2002).
[26] F. Li, L. Jin, Z. Xu, D. W. Wang, and S. J. Zhang, Appl. Phys. Lett. **102**, 152910 (2013).
[27] W. W. Cao and L. E. Cross, Phys. Rev. B **47**, 4825 (1993).
[28] Y. Ishibashi and M. Iwata, Jpn. J. Appl. Phys., Part 1 **38**, 800 (1999).
[29] D. Damjanovic, Appl. Phys. Lett. **97**, 062906 (2010).
[30] D. Damjanovic, J. Am. Ceram. Soc. **88**, 2663 (2005).
[31] J. Peng, H. S. Luo, D. Lin, H. Q. Xu, T. H. He, and W. Q. Jin, Appl. Phys. Lett. **85**, 6221 (2004).